Probing Glass Transition Temperature of Polymer Thin Films under Static Shear Stress

Dong Hyup Kim[†,‡,#], *Cindy Y. Chen*[†], *and Zahra Fakhraai*[†,*]

† Department of Chemistry, University of Pennsylvania, Philadelphia, Pennsylvania 19147, United States

‡ School of Chemical and Biological Engineering, Seoul National University, Seoul 08826, Republic of Korea

KEYWORDS glass transition, glass transition temperatures, polymer thin films, confinement, glasses

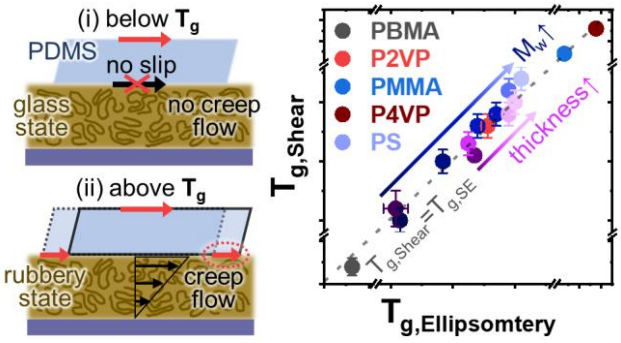

ABSTRACT

Accurate characterization of the glass transition temperature (T_g) in polymer thin films is pivotal for their application in nanotechnology. Here, we introduced a novel and simple method

to measure T_g based on the observation of creep flow in response to static shear stress. The technique employs a polydimethylsiloxane (PDMS) pad placed on top of the polymer thin film. The sample is held isothermally at 2 K intervals upon heating. At each temperature, steady shear is applied with constant normal and lateral forces for a constant duration of time. T_g is identified by the onset temperature where PDMS displacement is observed at the polymer/PDMS interface in optical microscopy. The measured T_gs strongly correlate with those measured by spectroscopic ellipsometry for various polymers with various molecular weights and film thicknesses. Furthermore, we demonstrate that this approach can be employed in conditions where T_g measurements using other methods may be challenging. For example, in polymer-infiltrated nanoparticle films (PINFs), the T_g of the highly confined polymer in the composite can be accurately measured. This facile and inexpensive technique can be readily adopted in various industries, where alternative techniques, such as ellipsometry, can be costly and require extensive expertise.

INTRODUCTION

Polymer thin films and composites can play an essential role in various fields of nanotechnology, such as lithography, [1] transistors, [2, 3] sensors, [4] energy harvesting devices, [5] material transfer, [6] nanotemplates, [7-10] and more. Generally, material properties of polymers are intricately related to the segmental motion of polymer chains, [11-13] which can strongly vary in glass forming polymers, depending on their glass transition temperatures (T_g). [14, 15]

In polymer thin films, T_g can strongly deviate from that of the bulk due to the strong perturbations of the free surface and substrate interfaces. [16-26] A strong interaction between polymer chains and the substrate can restrict the relaxation dynamics of polymer chains, which can propagate through the films, [27] thus changing the average film T_g. [28] Similarly, soft substrates have been shown to strongly modify polymer film T_g at distances exceeding 200 nm. [25] On the other hand, at their free surface, polymer films show enhanced relaxation dynamics[24, 26, 29, 30] compared to that of the bulk, which can result in dramatic T_g reduction. [17, 18, 21, 31] These effects can be long-range and affect polymer properties at distances 10-100 nm from each interface, depending on the mechanical properties of the substrate and the polymer chemistry.

Apart from the interfacial effects in thin films, numerous other factors, including additives, crosslinking, and residual solvents[32-34] can also influence T_g, making it difficult to estimate the effective T_g of polymer films for a desired application. Moreover, geometric confinement in highly loaded polymer nanocomposites[35] and nanoporous materials[36, 37] can also affect the T_g of polymers. In polymer-infiltrated nanoparticle films (PINFs), T_g can increase by as much as 50 K above the bulk T_g. [36 38, 39] As such, developing robust methods to measure T_g under

various conditions is important to advance our understanding of the complex factors affecting T_g, for predictive design of composite materials.

While measuring the effective T_g of polymer thin films is important, common techniques such as differential scanning calorimetry (DSC) are unsuitable for measuring the T_g of thin films or composite samples. The most popular methods of measuring thin films T_g are spectroscopic ellipsometry (SE) [16] and nano DSC, [40, 41] which are actively used in research settings. However, these techniques can be expensive and require technical expertise, limiting their broad use in industrial settings. As such, simple and easily accessible alternative methods can expand the utilization of T_g measurements in determining material properties. [42]

T_g of bulk and thin polymer films can also be measured through rheological measurements. Here, the viscoelastic response of a film can be measured upon applied shear stress at various times and temperatures. The system's response is typically observed to follow time-temperature superposition (TTS). [43] The resulting temperature-dependent shift factors are proportional to the polymer's relaxation time, which can then be used to obtain T_g. [44] Typically, dynamic T_g is defined as a temperature where the structural relaxation time (τ_α) is ~100 s, [19, 45] which corresponds to T_g measured by DSC or dilatometry[46-48] (including ellipsometry) at a cooling rate of 10 K/min. In bulk systems, the change of cooling rate by a factor of 10, typically results in 2-3 K change in T_g. [19] Accordingly, around the nominal T_g, the viscosity can vary by 3-4 decades in a small window of temperature (20-30 K), which is also measured as the breadth of the glass transition in DSC experiments. [19-21, 45] As such, the cooling-rate dependent T_g is generally proportional to the non-Arrhenius behavior of the relxation dynamics seen in rheological measurements, where the cooling rate is inversely proportional to the system's relaxation time at T_g . [49] In thin films, the average T_g is typically lower and the dependence of both the relaxation time and inverse cooling rate on temperature

has been observed to be weaker (lower fragility or activation energy), and the breadth of the glass transition is generally increased as the film thickness is decreased. [19, 21, 45] In addition, these effects typically starts only at slow cooling rates or slow relaxation times ($\tau_\alpha < 1$, or a temperature a few degrees above bulk T_g), above which minimal effects of film thickness is observed. [19, 21, 45] This is due to increased gradients of mobility across thin films, due to the interplay between the enhanced mobility of the free surface and the slower dynamics close to the substrate. [21] Nevertheless, previous studies have shown that the average T_g measured using ellipsometry at various cooling rates still corresponds to the averaged relaxation dynamics across the films. [19, 45]

In this study, we introduce a method to probe T_g of polymer thin films based on state-dependent creep flow under static shear stress, which is analogous to the TTS approach but with a simplification of using a constant measurement time. A static shear stress is applied to a thin polymer after placing a PDMS pad on the film's surface. Constant normal and lateral forces are simultaneously applied to the PDMS pad for a constant duration. Below the T_g, polymers have high viscosity, and their segmental relaxation is extremely slow. As such, creep flow is not observed at the polymer/PDMS interface at the time scale of the experiments. In contrast, above T_g, the viscosity is decreased dramatically (glass to rubber transition), [44, 50] and flow is observed at the polymer/PDMS interface. As such, the film T_g can be determined by measuring the distance over which the interface has moved as a function of temperature after some elapsed time. We demonstrate that by properly selecting the elapsed time, the measured $T_{g,Shear}$ highly correlate with the conventionally measured $T_{g,SE}$ values determined by spectroscopic ellipsometry (SE). The technique is validated for various polymers with various molecular weights and film thicknesses and in PINFs with various degrees of confinement.

RESULTS AND DISCUSSION

Determining T_g using applied shear. An overview of the experimental setup is illustrated in **Figure 1**. Quasi-static shear is applied using a polydimethylsiloxane (PDMS) pad similar to previous reports. [51-55] In this method, as shown in **Figure 1a**, a PDMS pad (10x10 mm^2 area, 1 mm-thick, preparation details in the experimental section) is placed on the surface of a polymer film deposited on a rigid silicon substrate. Under a steady normal force of $F_N = 4.9$ N, a lateral force of $F_S = 2.5$ N is applied to the top surface of the PDMS pad to generate a steady shear at various isothermal temperatures. The shear stress was calculated to be 25 kPa based on the values of the normal force, the lateral force, and the area covered by the PDMS pad (details in the experimental section and schemes in **Figure S1**). The magnitude of shear stress and the hold time were chosen such that a flow (*i.e.* the displacement of the polymer/PDMS interface) would be optically observed just above T_g. During the glass to rubber transition, the viscosity of a polymer film typically changes by 3-4 decades from a few GPa.s to a few MPa.s. [38, 50] At constant applied stress, this difference can either be probed by changing the measurement time, which is experimentally impractical given the, or by choosing a constant wait time while varying the experimental temperature (typically in a 20-30 K window breadth of T_g), [19, 20] which is the approach taken here. For example, a typical wait time of 30 min was chosen for the experiments. To observe a 1-μm-displacement, the detection limit under the optical microscope, a minimum shear rate of ~0.5×10^{-3} s^{-1} is needed. In the rubbery state with a viscosity of 10^6 Pa.s, ~5 kPa of minimum shear stress is needed to observe displacement, while in the glass state with a viscosity of 10^9 Pa.s, at least ~500 kPa would be needed. Thus, the selected 25 kPa of shear stress can only form optically visible creep above T_g. We also note that to observe a flow under the microscope, measurements require wait times longer than the polymer's reptation time, [56] which were also considered, as

detailed further below. Furthermore, this amount of shear stress is sufficient to make all polymer chains across the thickness direction[57] experience terminal flow reflecting the average relaxation response of the film, even if there is a mobility gradient from the pad to the substrate.

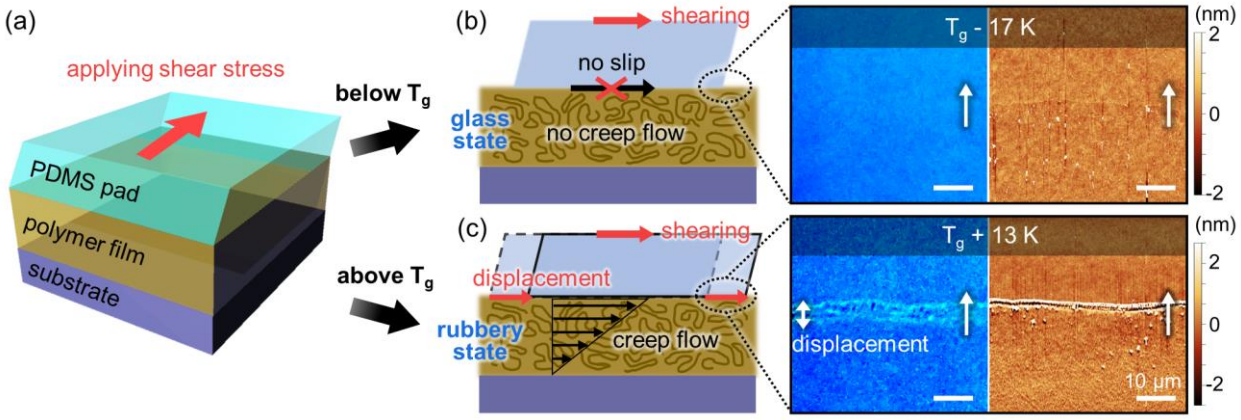

Figure 1. State-dependent creep flow of polymer thin films under static shear stress. (a) Schematic illustration of a polymer thin film sandwiched between a rigid substrate and a PDMS pad under applied steady shear. (b, c) From left to right, schematic illustration, optical microscope images, and AFM height images of (b) the glass/PDMS interface (at 353 K, below T_g) and (c) the rubber/PDMS interface (at 383 K, above T_g) of a 115-nm-thick PS film (M_w=99 kg/mol) held for 30 min under 25 kPa of applied shear stress. White and red arrows indicate the direction of shear. Scale bars are 10 μm. The lateral features observed in the microscope and AFM images in (c) indicate displacement of the PDMS at the PDMS/polymer interface above T_g.

Figures 1b and **1c** show that when a shear stress of 25 kPa is applied to a 115 nm film of polystyrene (PS, M_w = 99 kg/mol) for a duration of 30 min at two different temperatures, 353 K and 383 K, PS films showed different surface features in optical microscopy (OM) and atomic force microscopy (AFM) At 383 K, which is above T_g (**Figures 1c**), a creep flow is

observed in the direction of shear at the PS/PDMS interface, while no discernible features are seen at 353 K (below T_g). This is because when the static shear stress is applied to the PDMS surface, momentum is transferred to the rubbery polymer film, resulting in a creep flow in the direction of shear (schematically shown in **Figure 1c**). Below T_g, the relaxation time of the polymer is too long, and in the absence of any slippage, creep flow is not observed in the duration of the experiment at the polymer/PDMS interface (schematically shown in **Figures 1b**)

To accurately determine $T_{g,Shear}$, the displacement distance of the PDMS pad after applying a steady shear stress of 25 kPa for 30 min was measured by holding the sample isothermally at a fixed temperature. To cover the broad range of temperatures, separate shear experiments were conducted for individual samples of the same condition at different temperatures at 2 K intervals. At each temperature, the sample was held under shear for 30 min. We note that the thermal expansion of PDMS, even in the absence of applied shear stress, can move the position of the PDMS footprint at each temperature. To accurately determine the displacement distance due to the applied shear stress, the displacement induced by the thermal expansion of the PDMS pad, measured separately in the absence of external shear (OM images and schemes in **Figure S2**), was deducted from the measured displacements under the applied shear. Please see the details in the experimental section and schemes in **Figure S1** and **Figure S2**. **Figure 2a** shows a plot of the calculated displacement of the PDMS due to external shear as a function of temperature for the 115-nm-thick film of PS (99 kg/mol). The corresponding OM images are shown in **Figure 2b**. $T_{g,Shear}$ was determined as the mid-temperature between the temperatures at which displacement was first observed and the highest temperature where no apparent displacement was observed (**Figure 2a** inset). As seen in **Figure 2a**, under the conditions used here, the displacement of the PDMS pad was first observed at 371 K. Upon further heating, the

displacement increased dramatically, indicating significant viscosity reduction at higher temperatures. The onset temperature of displacement increment ranged between 371 K and 373 K for various samples in independent experiments. As such, the $T_{g,Shear}$ of this film thickness was determined to be $T_{g,Shear}$ = 372 ± 2 K, as shown in the inset of **Figure 2a.** For films of the same thickness, SE measurements show $T_{g,SE}$ = 370 ± 2 K, as shown in **Figure 2a** (experimental details in Materials and Methods).

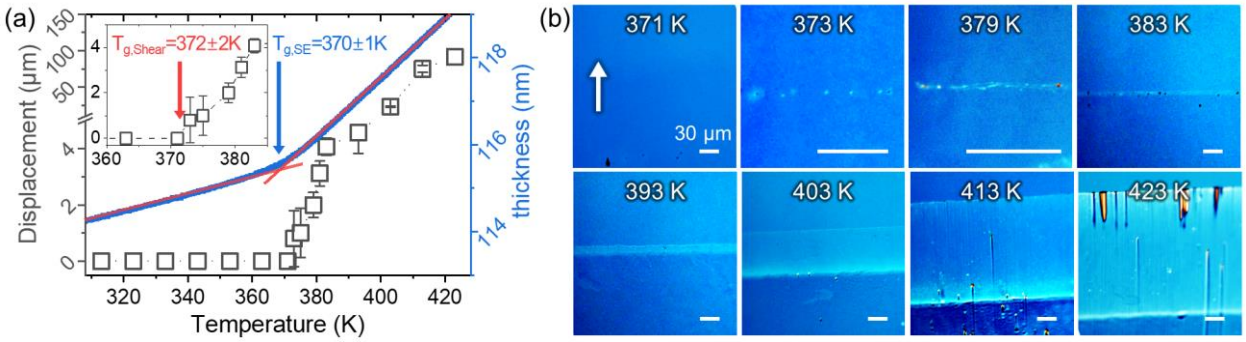

Figure 2. Probing $T_{g,Shear}$ of polymer thin films based on the displacement of the PS/PDMS interface after applying a steady shear stress at various temperatures. (a) Displacements of the PDMS edge on the PS(115 nm, 99 kg/mol)/PDMS interface vs. temperature, after applying 25 kPa of steady shear stress for 30 min (black squares, left axis), and thickness change vs. temperature monitored using spectroscopic ellipsometry (blue dots, right axis). $T_{g,Shear}$ = 372 ± 2 K is determined as the midpoint of temperatures below and above which displacement was first observed (red arrow in the inset), and $T_{g,SE}$ = 370 ± 1 K is determined as the intersection of two linear fits (red lines) to the film expansion in the glass and supercooled liquid states (blue arrow). (b) Optical microscope images at various temperatures after the applied shear show the displacement (or lack thereof) of the PDMS edge at the PS/PDMS interface. The white arrow indicates the direction of shear. Scale bars are 30 μm.

The role of polymer molecular weight in the measured $T_{g,Shear}$ values. Notably, the apparent $T_{g,Shear}$ of the PS film ($T_{g,Shear}$= 372 ± 2 K) is slightly higher than the T_g obtained from SE ($T_{g,SE}$ = 370 ± 1 K). As discussed above, given the strong dependence of viscosity on temperatures, the applied shear, as well as the shearing time, can affect the value of $T_{g,Shear}$. The shearing method fundamentally relies on measuring a displacement larger than the optical resolution limit. However, even when an objective lens with a high numerical aperture (NA) value is used, the maximum resolution is only a few hundred nanometers. As such, the chosen 30 min of shearing is insufficient to allow identifiable displacement lengths at the dilatometric ($T_{g,SE}$) for the PS thin films with a high molecular weight of M_w = 99 kg/mol, which is larger than the entanglement molecular weight, M_e. [58]

To further demonstrate the role of molecular weight in determining $T_{g,Shear}$, measurements were performed on 110-nm-thick PS films of various molecular weights. **Figure 3a** shows the measured T_g values using both methods as a function of molecular weights. The corresponding OM images are shown in **Figure S3**. As seen in this figure, as M_w is increased beyond M_e, a small but systematic difference is observed between $T_{g,Shear}$, and $T_{g,SE}$. However, we note that T_g measured by both methods follows the Fox-Flory relation, **eq 1**. [59]

$$T_g = T_g^{\infty} - \frac{C}{M_w} \tag{1}$$

The red and black solid lines in **Figure 3a** correspond to fitted curves with $T_{g,SE}^{\infty}$ = 371 ± 1 K and C_{SE} = 92.5 ± 2.0 mol.K/kg, and $T_{g,Shear}^{\infty}$ = 373 ± 2 K and C_{Shear} = 106.6 ± 6.0 mol.K/kg, respectively. It should be noted that within the error, the fitting constant C for both methods was close to the previously reported value of C = 100 mol.K/kg for PS. [59]

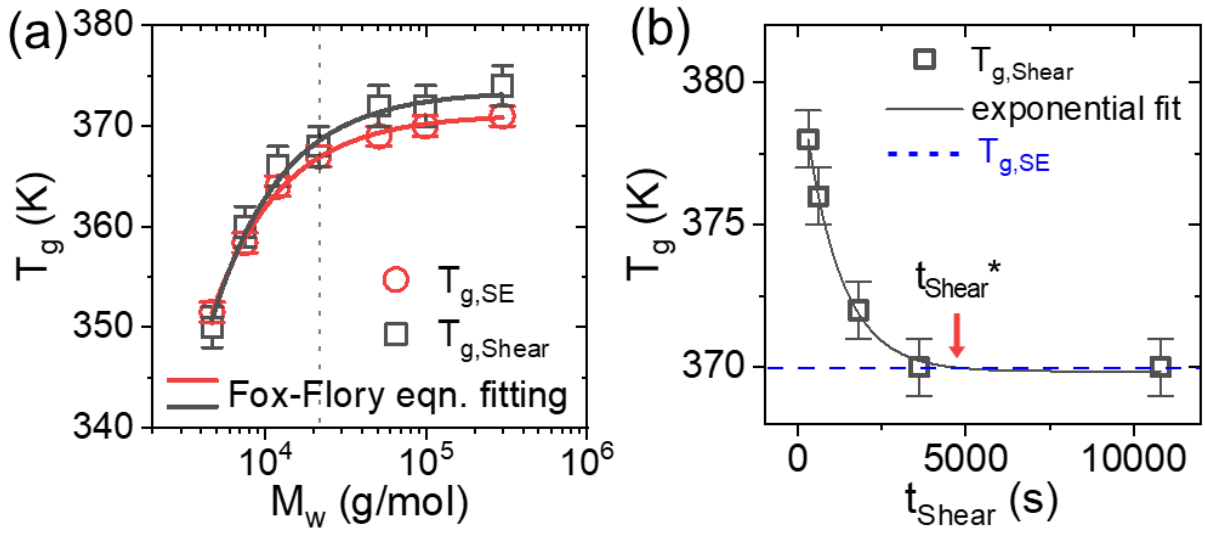

Figure 3. Comparison of $T_{g,Shear}$ (black squares) and $T_{g,SE}$ (red circles) as a function of M_w. (a) $T_{g,Shear}$ (black squares) and $T_{g,SE}$ (red circles) vs. M_w for 110-nm-thick PS films of various molecular weights. The black dotted line indicates M_e. (b) $T_{g,Shear}$ vs. shearing time, upon applying 25 kPa of shear stress for 115-nm-thick PS(99 kg/mol) films.

The larger value of $T_{g,Shear}^{\infty}$ compared to $T_{g,SE}^{\infty}$ agrees that the 30 min shearing time was insufficient for T_g determination at the applied normal load and the OM detection resolution used in this study. As seen in **Figure 3a**, the discrepancy between the two T_g values increases with molecular weight (also seen in the plot of ΔT_g vs. M_w in **Figure S4**) due to the rapid increase in the film viscosity as M_w is increased to above the entanglement threshold. Below M_e, the film viscosity is low enough for 30 min hold time to yield an accurate measure of $T_{g,Shear}$, and for the two methods to agree well.

To determine the critical shearing time, t_{Shear}*, required to achieve a relatively time-independent $T_{g,Shear}$, the dependence of $T_{g,Shear}$ on t_{Shear} was explored in 115 nm PS films with M_w = 99 kg/mol. As seen in **Figure 3b** (OM images for each sample in **Figure S5**), increasing t_{Shear} decreases $T_{g,Shear}$ until a plateau is achieved for holding times longer than

3000 s (50 min). To explain this trend, we note that to observe the creep flow in addition to the glass to rubber transition, the wait time needs to be long enough to account for the reptation of the polymer chains. As such, larger T_g differences as observed at higher at higher molecular weights. We noted that $T_{g,Shear}$ can be lowered when the observation time is exponentially increased, given the super-Arrhenius behavior of viscosity near the glass transition. The solid line in **Figure 3b** is an exponential fit of $T_{g.Shear}\ (K) = 369.85e^{-t_{Shear}/1081}$ further demonstrating that $T_{g,Shear}$ indeed decays exponentially as a function of t_{shear}. To obtain accurate $T_{g,Shear}$, t_{Shear} should be longer than the $t^*_{Shear} = (5 \pm 2)10^3 s$. t_{shear}* can be considered as when the polymer chains' total reptation distance becomes as long as optically visible length, e.g. 1μm, right above the T_g of polymer thin films. This can be expressed in this way: $t^*_{Shear} = (\frac{1000\ \text{nm}}{R_g})t_{rep}$, where R_g and t_{rep} are the radius of gyration and reptation time at T_g, respectively. This equation also shows the relation between t_{shear}* and the longest relaxation time (t_{rep} in this case). [56]

The application of the shearing method in determining $T_{g,shear}$. The shearing method to measure $T_{g,Shear}$ can be applied broadly to various polymeric systems, film thicknesses, and composite materials. Further validation of the shearing method was made using various types of glassy polymers. OM images in **Figure S6** shows the measured $T_{g,shear}$ values for various polymers (values listed in **Table S1**). **Figure 4b** shows a strong correlation between $T_{g,Shear}$ and $T_{g,SE}$ values, demonstrating the reliability of the shearing technique.

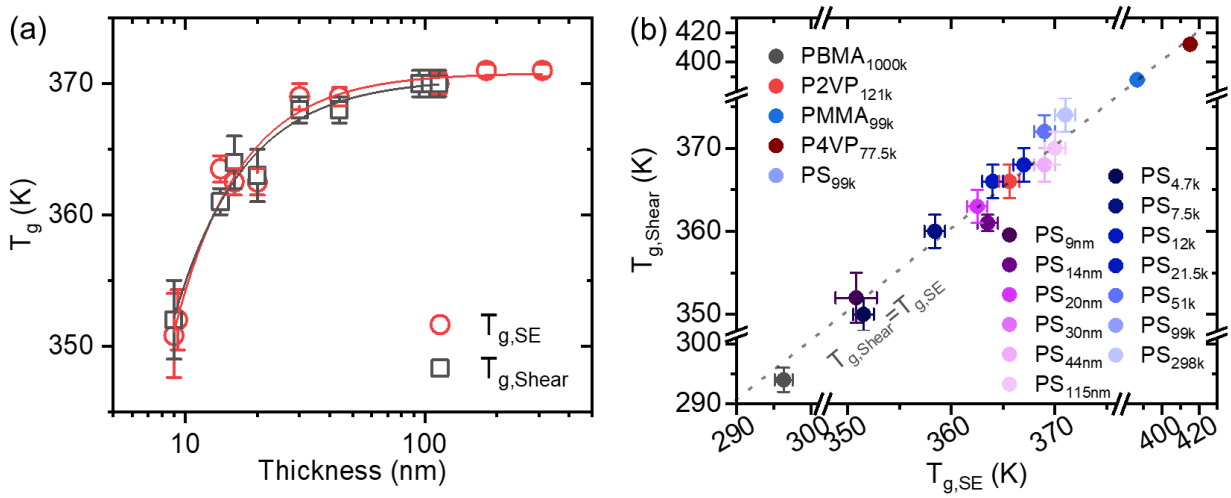

Figure 4. (a) $T_{g,Shear}$ (black squares) and $T_{g,SE}$ (red circles) as a function of film thickness of PS(99 kg/mol) thin films. The solid lines are guides for the eye. (b) The plot of T_g for various polymer thin films. The dotted line is a guideline where $T_{g,Shear}$ and $T_{g,SE}$ are identical.

This method shows a similar degree of accuracy in measurements of T_g in PS thin films on Si/SiO_2, where T_g decreases with film thickness (**Figure 4a** and **Figure S7** for the corresponding OM images). As shown in **Figure 4a,** both $T_{g,Shear}$ and $T_{g,SE}$ show ~18 K reduction as the film thickness is decreased to ~9 nm, with a strong correlation between the two methods, as seen in **Figure 4b**.

It is important to note that the $T_{g,Shear}$ values obtained based on samples covered by PDMS at the surface are consistent with the $T_{g,SE}$ measured without the top PDMS layer, as well as previously measured values of T_g reduction in PS thin films with free surfaces on Si/SiO_2 substrates (about 25 K T_g reduction for 8-nm-thick PS(136 kg/mol) films). [19] In contrast, previous measurements had shown much more pronounced T_g reduction effects for PS films deposited on PDMS substrates. [22] As such, one would expect a relatively large contribution to T_g when PDMS is placed on the PS surface. There are two possible reasons for these apparent

differences. Roth and coworkers have shown that [25, 60] to observe a large interfacial effect at the PDMS/PS interface, thermal annealing is needed to allow the polymers to mix and interlock at the interface. Similarly, previous studies have shown that even when a rigid top layer such as aluminum is used or multiple PS layers are stacked, the details of interface preparation and annealing can affect whether or not T_g reduction is observed. [60, 61] In the current shearing system, the absence of additional annealing ensures that the PDMS pad does not strongly interact with the free surface as previously reported, [25] and, as such, does not show the significant T_g reduction due to the PDMS interfacial effects. In addition, in the experiments here, the PDMS was placed on the surface of each film after the set temperature was reached to avoid effects due to interfacial annealing. [25] Furthermore, a recent study[62] also explored creep behavior at slow shear rates where ultrathin film's T_g reduction is amplified. These experiments also do not see any additional T_g reduction induced by the PDMS interfacial effects. Therefore, the overlap of two fitting curves from SE and the shearing method, along with highly similar T_g^{bulk} values, validates that the shearing method can be used to explore the effect of free surfaces on T_g values in ultra-thin films.

We also note that previous studies have shown the important effect of the rate of relaxation or the cooling rate in observing T_g reduction in thin polymer films, where at high cooling rates or fast relaxation rates (faster than 1 second), the surface-induced T_g reduction becomes negligible The observed similarity between the $T_{g,Shear}$ and $T_{g,SE}$ in ultra-thin films is also because shearing experiments are performed at steady and slow shear rates, where the enhanced surface mobility is significant. In contrast, most dielectric-relaxation/calorimetric measurements, [46-48] or measurements of surface shear relaxation using AFM probe time scales faster than 1 second, and as such do not see such significant effects from the free surface. [47, 63]

Another demonstration of the utility of the shearing method in determining T_g, is in highly confined polymers within polymer-infiltrated nanoparticle films (PINFs). **Figure 5a** illustrates the process of producing PINFs by capillary rise infiltration of polymers into a nanoparticle film, resulting in an exceptionally high nanoparticle loading density (*c.a.* 65 vol%). The details for the in-situ SE and PINF preparation are given in the experimental section in supporting information, the fitted results of in-situ SE data in **Figure S8** and **Figure S9**. Previous studies[36, 38] have demonstrated that viscosity and T_g of polymers in PINFs are dramatically increased due to the extreme nanoconfinement effects on the polymer chains.

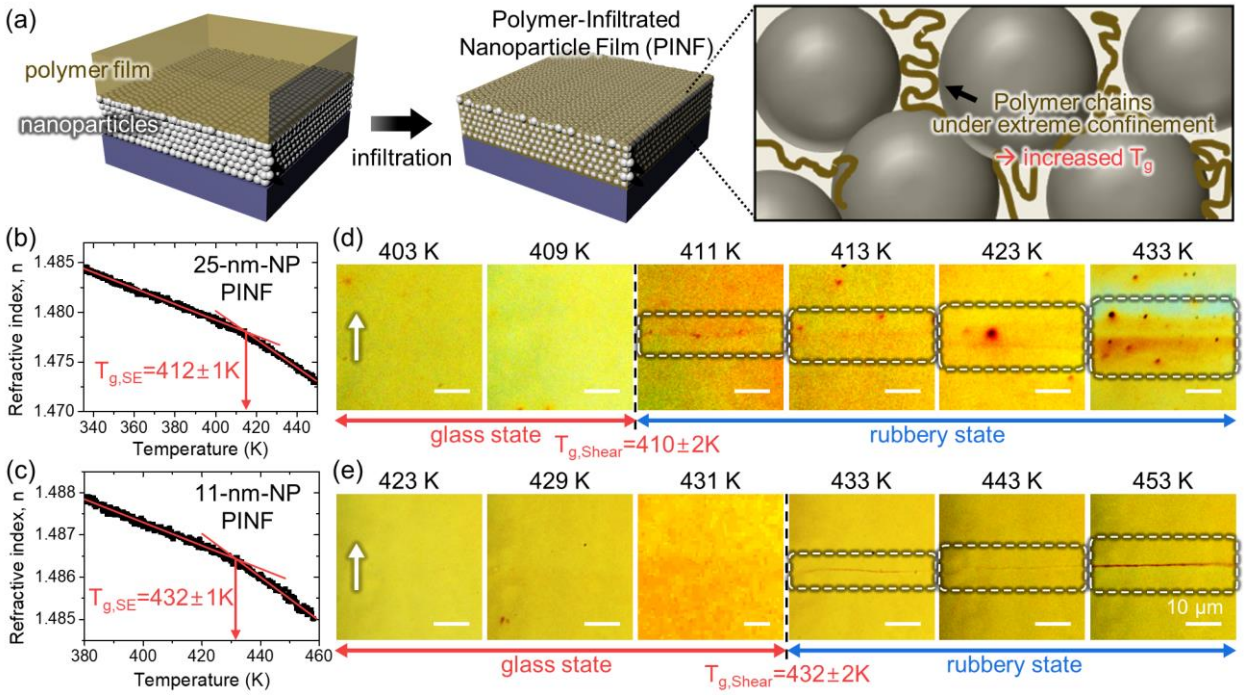

Figure 5. T_g measurements of polymer-infiltrated nanoparticle films (PINF). (a) Schematic illustration of a PINF with high nanoparticle (NP) loading. The plots of temperature-dependent refractive index change of PS(298 kg/mol)/SiO_2 PINFs in (b) films with 25-nm diameter NPs and (c) 11-nm-diamter NPs. The optical microscope images in (d) and (e) show the displacements of the PDMS edge after applying shear stress (25 kPa for 30 min ~ 1 H) to

PS(298 kg/mol)/SiO_2 PINFs with (d) 25-nm-diamter NP films and (e) 11-nm-diameter NP films, respectively. The white arrow indicates the shear direction.

The PS(298 kg/mol)-based 25-nm-sized nanoparticle (25-nm-NP) PINF and 11-nm-NP PINF were prepared using the previously reported method. The changes in the refractive index, *n*, depending on temperature were monitored to measure the $T_{g,SE}$, as shown in **Figure 5b and c**. The $T_{g,SE}$ of the 25-nm-NP PINF and 11-nm-NP PINF were determined to be 412 ± 1 K and 432 ±1 K, respectively. In general, the smaller nanoparticles in PINFs give the polymer a higher level of nanoconfinement and show greater T_g enhancement. Thus, the T_g increments for the 25-nm-NP PINF and 11-nm-NP PINF were 42 K and 62 K compared to the bulk T_g of PS(298 kg/mol), respectively.

The $T_{g,Shear}$ of both 25-nm-NP PINF and 11-nm-NP PINF were measured by the shearing method in **Figure 5d and e**, respectively. The nanoparticles-only films were deformed by the static shear stress of the PDMS pad and showed displacement footprint from the PDMS pad at all temperatures, as shown in the OM images of **Figure S10**. However, after the infiltration of polymers into the nanoparticle films, the displacement footprint from the PDMS pad was observed only at temperatures higher than the T_g of the confined polymers, as shown in the right four columns of **Figure 5d and e**. The $T_{g,Shear}$ were 410 ± 2 K and 432 ± 2 K for 25-nm-NP PINF and 11-nm-NP PINF, respectively, corresponding with the $T_{g,SE}$. These results confirmed the capability of the shearing method to measure the T_g of highly confined polymer chains, such as the T_g of PINF, as well as general polymer thin films shown in **Figure 4b**.

Previous studies have shown that in PINF systems, the chain length is not important in the observed T_g increases. Instead, the confinement in these systems is mostly due to local restrictions in the segmental relaxations. [38, 64, 65] In addition, studies on the molecular weight

dependence of the viscosity in these systems shows non-monotonic changes indicating reduced entanglement density. As such, strong changes in the reptation time of the polymer are not expected to play a significant role. The observed increases in $T_{g,Shear}$ in this study, which reasonably correlate with the variation in $T_{g,SE}$ indicates that the 1 H shearing time was adequate to properly observe the flow due to glass transition. We note that the mechanism of this correlation is not immediately clear, as the rigid network of the nanoparticle likely prevents the entire film from shearing. Instead, we hypothesize that the polymer expansion produces an intermediate layer that can then be sheared through the process. We have previously demonstrated that the expansion of the polymer film can indeed be also observed in SE experiments through measurements of the top layer thickness[38] with a second apparent $T_{g,SE}$ that corresponds to that of the composite thickness. A more detailed study of the detailed phenomenon is outside the scope of the current manuscript and will be examined in the future.

CONCLUSIONS

In summary, this study explores the creep flow of polymer thin films in response to an applied static shear stress below and above the glass transition temperature to demonstrate that such measurements can be used as a facile approach to probing the T_g of polymer thin films, prepared under various conditions. In this approach, static shear stress is applied to polymer thin films by applying normal and lateral forces on a PDMS pad placed on the film's free surface. The displacement of the PDMS on the polymer/PDMS interface is only observed when the temperature is raised above the film's T_g. T_g is then determined at the transition temperature where the PDMS displacement footprint is observed in optical microscopy after an adequately long elapsed time, determined by the polymer's creep flow. The choice of the elapsed time can be optimized, in a manner that is analogous to variations

of the cooling rate in conventional T_g measurements and is expected to be inversely correlated. In entangled polymer systems, this time will also depend on the reptation time of the polymer. A strong correlation is observed between the T_g values obtained by the shearing method and those of ellipsometry for various polymers and at various molecular weights, film thicknesses, and polymer nanocomposites, confirming the general feasibility of this method. This relatively inexpensive method can be reliably used in systems with complicated geometries, such as polymer thin films or polymer infiltrated nanoparticle films, where conventional methods such as ellipsometry require sufficient signal or sophisticated modeling, enabling widespread adaptation in various applications.

EXPERIMENTAL SECTION

Materials

Polystyrene (PS), poly(n-butyl methacrylate) (PBMA), poly(2-vinyl pyridine) (P2VP), polymethyl methacrylate (PMMA), and poly(4-vinyl pyridine) (P4VP) were purchased from Polymer Source, Inc. The molecular weights of PS were 4.7 kg/mol (polydispersity index (PDI) = 1.06), 7.5 kg/mol (PDI = 1.06), 12 kg/mol (PDI = 1.02), 21.5 kg/mol (PDI = 1.02), 51 kg/mol (PDI = 1.03), 99 kg/mol (PDI = 1.06), and 298 kg/mol (PDI = 1.15). The molecular weight of PBMA was 1,000 kg/mol (PDI = 1.4). The molecular weight of P2VP was 121 kg/mol (PDI = 1.07). The molecular weight of PMMA was 99 kg/mol (PDI = 1.12). The molecular weight of P4VP was 77.5 kg/mol (PDI = 1.05). Toluene (Sigma-Aldrich, anhydrous, 99.8 %) and 1-butanol (Sigma-Aldrich, 99 %) were used in this study. ⟨100⟩ Si wafers (purchased from Virginia Semiconductor) were employed as substrates. Silica nanoparticles (NPs) with diameters of 11 nm (Organosilicasol IPA-ST, 30 – 31 wt% suspension in isopropanol, Nissan Chemical American Cooperation) and 25 nm (LUDOX TM-50, 50 wt% suspense on in water, Sigma Aldrich) were used. Sylgard 184 (Dow Corning) was used for PDMS pad preparation.

Sample Preparation

PS, PBMA, P2VP, PMMA, and P4VP were spin-coated on the Si substrates from toluene solution (0.3–1.5 wt%) for PS, PBMA, and PMMA and from 1-butanol solution (1–1.5 wt%) for P2VP and P4VP. The film thicknesses were measured using a spectroscopic ellipsometer (M-2000V, J.A. Woollam Co.). All polymer films were thermally annealed at a temperature at least 30 K above their respective T_g for 24 H under vacuum to erase the thermal history of the films.

The PDMS pads were prepared from Sylgard 184 (Dow Corning) at a 10:1 ratio of base to curing agent and were cured at 323 K for 12 H in ambient conditions. The cross-linked PDMS pads were roughly 1-mm-thick and were cut into 10x10 mm pieces. Pads were placed on the polymer film surfaces without further annealing.

Preparation of PINFs

200-nm-thick films of randomly-packed silica NPs of various diameters were generated by spin coating NP solutions onto silicon wafers. The films were then annealed at 773 K for 30 minutes under ambient conditions to remove excess solvent and stabilize the NP films. After annealing, 78 nm layers of PS(298 kg/mol) were spin coated on top of the NP films to generate bilayer films. The bilayer films were then heated at 453 K in the vacuum oven to remove the solvent and allow PS to infiltrate into the NP pores. The resulting bilayer thicknesses were determined by Spectroscopic Ellipsometry (SE). All the prepared PINFs were fully infiltrated with PS, with less than 3 nm top residual layers.

Static Shear Stress Measurements using Optical Microscopy

Static shear stress was applied to polymer thin films using a homemade shearing stage equipped with a Linkam temperature-controlled stage (Linkam THMS600). The overall experimental procedures are schematically shown in **Figure S1**. Each sample was placed on the pre-heated Linkam stage to reach the desired experimental temperature. A PDMS pad was then placed on

the sample. After 1~3 minutes of hold to ensure the thermal equilibration and expansion of PDMS, two weight blocks were placed on the PDMS pad to simultaneously apply a lateral and a normal force to the sample. The shear stress was controlled by changing the applied lateral force and the area of the PDMS pad. Most reported experiments were performed by applying 25 kPa shear stress (a normal force of 4.9 N and a lateral force of 2.5 N to the 10x10 mm sized PDMS pad), and steady shear was applied for 30 min to measure whether a displacement was observed in reflectance optical microscopy. Olympus Digital Microscope (BX51) was used to detect the motion of the PDMS on the PDMS/polymer surface by taking images of the PDMS pad footprint from separate individual experiments at every temperature of interest. Objective lenses with magnifications of x20, x50, and x100 with numerical aperture (NA) values of 0.4 ~ 0.5 were used.

In-situ Spectroscopic Ellipsometry (SE) T_g Measurements

A spectroscopic ellipsometer (SE, M-2000V, J.A. Woollam) equipped with a Linkam temperature-controlled stage (Linkam THMS600) was used for T_g measurements. The raw SE data, $\Psi(\lambda)$ and $\Delta(\lambda)$, were measured in the spectroscopic range of $600 < \lambda < 1600$ nm at ambient conditions and were fit to a model consisting of a temperature-dependent model for silicon substrate, a 1 nm native oxide layer, and a Cauchy layer for the polymer film. The index of refraction of the Cauchy layer was modeled as $n = A + \frac{B}{\lambda}$, where A and B were the fitting parameters, along with the film thickness h. Once an initial fit was performed at room temperature, only A and h were fitted during the subsequent *in situ* heating and cooling cycles. $T_{g,SE}$ was measured upon cooling at a cooling rate of 10 K/min. $T_{g,SE}$ was determined as the cross point between two linear fits, which were fitted upper and lower temperature ranges in a 30 K window, as shown in **Figure 2a**. $T_{g,SE}$ was validated by comparing at least three heating and cooling cycles.

For modeling PINFs, an additional Cauchy layer was considered for the composite layer at the bottom. For these films, the thickness of the NP layer was held constant while fitting the thickness of the PS top layer and the indices of refraction of both layers. To monitor the infiltration of the PS in bilayer films at a constant temperature, before T_g measurements, a 3rd Cauchy layer was also considered, where from the bottom to the top, an empty NP layer, a composite layer, and a top residual PS layer were considered (more details in fitting results of in-situ SE data in **Figure S8** and **Figure S9**).[1] During the first heating ramp to 453 K at a heating rate of 30 K/min, the bilayer was held at the temperature for about 30 min to let PS infiltrate into the NP pore. When the top PS layer thickness or the n of the bottom NP layer became constant, it indicated complete PS infiltration into NP pores. After this step, the residual top layer became too thin, which was not modeled. Then, the T_g of the PS-infiltrated nanoparticle layer was measured by monitoring the changes in the index of refraction of the composite layer vs. temperature upon cooling at a cooling rate of 10 K/min.

Atomic Force Microscopy

Bruker Dimension Icon atomic force microscope (AFM) was used. AFM images were collected in tapping mode with Tap300Al-G tips (Budget Sensors, 10 nm tip radius of curvature). The image resolution was 512 x 512 points, and the images were obtained at a scan rate of 1 Hz. Microscope images were processed using the Gwyddion software.

ASSOCIATED CONTENT

Supporting Information

The Supporting Information is available free of charge at

Schematic illustration of experimental procedures; PDMS displacement footprint due to

thermal expansion of PDMS (without external shear forces); PDMS displacement footprint on PS thin films of various molecular weights; Molecular weight-dependent T_g differences between SE and shearing methods; PDMS displacement footprint on PS thin films for various shearing durations; Table of T_g for various polymer thin films; PDMS displacement footprint on various polymer thin films; PDMS displacement footprint on PS thin films in various thicknesses; Details for the in-situ Spectroscopic Ellipsometry (SE) for PINF; The goodness of the fit for the in-situ Spectroscopic Ellipsometry (SE) for PINF; Nanoparticle-only films after applying static shear stress (PDF)

The source data are also available via Figshare at https://doi.org/10.6084/m9.figshare.26073427

AUTHOR INFORMATION

Corresponding Author

Zahra Fakhraai − Department of Chemistry, University of Pennsylvania, Philadelphia, Pennsylvania 19147, United States; orcid.org/0000-0002-0597-9882; Email: fakhraai@sas.upenn.edu

Authors

Dong Hyup Kim − Department of Chemistry, University of Pennsylvania, Philadelphia, Pennsylvania 19147, United States; School of Chemical and Biological Engineering, Seoul National University, Seoul 08826, Republic of Korea; orcid.org/0000-0003-3866-1878

Cindy Y. Chen − Department of Chemistry, University of Pennsylvania, Philadelphia, Pennsylvania 19147, United States; orcid.org/0000-0001-7401-3638

Present Addresses

Department of Chemistry, University of Chicago, Chicago, Illinois 60637, United States

Notes

The authors declare no competing financial interest.

ACKNOWLEDGMENT

This research was supported by the University of Pennsylvania Materials Research Science and Engineering Center (MRSEC, grant DMR-2309043). Partial support was provided by the Wisconsin MRSEC grant (DMR-2309000). D. H. K. acknowledges support from the National Research Foundation of Korea (NRF) grant funded by the Korean government (MSIT) (NRF-2021R1C1C2012905). C.Y.C. acknowledges support from the NSF Graduate Research Fellowship Program (NSF GRFP, DGE-1845298).

REFERENCES

1. Vieu, C.; Carcenac, F.; Pépin, A.; Chen, Y.; Mejias, M.; Lebib, A.; Manin-Ferlazzo, L.; Couraud, L.; Launois, H., Electron beam lithography: resolution limits and applications. *Appl. Surf. Sci.* **2000,** *164*, 111-117.

2. Kim, C.; Facchetti, A.; MARKS, T. J., Polymer Gate Dielectric Surface Viscoelasticity Modulates Pentacene Transistor Performance. *Science* **2007,** *318*, 76-80.

3. Kim, C.; Facchetti, A.; Marks, T. J., Probing the Surface Glass Transition Temperature of Polymer Films via Organic Semiconductor Growth Mode, Microstructure, and Thin-Film Transistor Response. *J. Am. Chem. Soc.* **2009,** *131*, 9122-9132.

4. Adhikari, B.; Majumdar, S., Polymers in sensor applications. *Prog. Polym. Sci.* **2004,** *29*, 699-766.

5. Shanbedi, M.; Ardebili, H.; Karim, A., Polymer-based triboelectric nanogenerators: Materials, characterization, and applications. *Prog. Polym. Sci.* **2023,** *144*, 101723.

6. Gurarslan, A.; Yu, Y.; Su, L.; Yu, Y.; Suarez, F.; Yao, S.; Zhu, Y.; Ozturk, M.; Zhang, Y.; Cao, L., Surface-Energy-Assisted Perfect Transfer of Centimeter-Scale Monolayer and Few-Layer MoS_2 Films onto Arbitrary Substrates. *ACS Nano* **2014,** *8*, 11522-11528.

7. Kim, D. H.; Kim, S. Y., Self-Assembled Copolymer Adsorption Layer-Induced Block Copolymer Nanostructures in Thin Films. *ACS Cent. Sci.* **2019,** *5*, 1562–1571.

8. Kim, D. H.; Suh, A.; Park, G.; Yoon, D. K.; Kim, S. Y., Nanoscratch-Directed Self-Assembly of Block Copolymer Thin Films. *ACS Appl. Mater. Interfaces* **2021,** *13*, 5772–5781.

9. Bae, S.; Kim, D. H.; Kim, S. Y., Constructing a Comprehensive Nanopattern Library through Morphological Transitions of Block Copolymer Surface Micelles via Direct Solvent Immersion. *Small* **2024,** *n/a*, 2311939.

10. Kim, D. H.; Kim, S. Y., Air–Water Interfacial Directed Self-Assembly of Block Copolymer Nanostrand Array. *Adv. Mater. Interfaces* **2022,** *9*, 2200660.

11. O'Connell, P. A.; McKenna, G. B., Rheological Measurements of the Thermoviscoelastic Response of Ultrathin Polymer Films. *Science* **2005,** *307*, 1760-1763.

12. Ding, Y.; Ro, H. W.; Germer, T. A.; Douglas, J. F.; Okerberg, B. C.; Karim, A.; Soles, C. L., Relaxation Behavior of Polymer Structures Fabricated by Nanoimprint Lithography. *ACS Nano* **2007,** *1*, 84-92.

13. Lee, J.-H.; Chung, J. Y.; Stafford, C. M., Effect of Confinement on Stiffness and Fracture of Thin Amorphous Polymer Films. *ACS Macro Lett.* **2012,** *1*, 122-126.

14. Ferry, J. D.; Parks, G. S., Studies on Glass XIII. Glass Formation by a Hydrocarbon Polymer. *J. Chem. Phys.* **1936,** *4*, 70-75.

15. Dudowicz, J.; Freed, K. F.; Douglas, J. F., Entropy theory of polymer glass formation revisited. I. General formulation. *J. Chem. Phys.* **2006,** *124*, 064901.

16. Keddie, J. L.; Jones, R. A. L.; Cory, R. A., Size-Dependent Depression of the Glass Transition Temperature in Polymer Films. *Europhys. Lett.* **1994,** *27*, 59.

17. Forrest, J. A.; Dalnoki-Veress, K.; Stevens, J. R.; Dutcher, J. R., Effect of Free Surfaces on the Glass Transition Temperature of Thin Polymer Films. *Phys. Rev. Lett.* **1996,** *77*, 2002-2005.

18. Ellison, C. J.; Torkelson, J. M., The distribution of glass-transition temperatures in nanoscopically confined glass formers. *Nat. Mater.* **2003,** *2*, 695–700.

19. Glor, E. C.; Fakhraai, Z., Facilitation of interfacial dynamics in entangled polymer films. *J. Chem. Phys.* **2014,** *141*, 194505.

20. Glor, E. C.; Composto, R. J.; Fakhraai, Z., Glass Transition Dynamics and Fragility of Ultrathin Miscible Polymer Blend Films. *Macromolecules* **2015,** *48*, 6682-6689.

21. Glor, E. C.; Angrand, G. V.; Fakhraai, Z., Exploring the broadening and the existence of two glass transitions due to competing interfacial effects in thin, supported polymer films. *J. Chem. Phys.* **2017,** *146*, 203330.

22. Baglay, R. R.; Roth, C. B., Local glass transition temperature $T_g(z)$ of polystyrene next to different polymers: Hard vs. soft confinement. *J. Chem. Phys.* **2017,** *146*, 203307.

23. Lee, H.-N.; Paeng, K.; Swallen, S. F.; Ediger, M. D., Direct Measurement of Molecular Mobility in Actively Deformed Polymer Glasses. *Science* **2009,** *323*, 231-234.

24. Paeng, K.; Swallen, S. F.; Ediger, M. D., Direct Measurement of Molecular Motion in Freestanding Polystyrene Thin Films. *J. Am. Chem. Soc.* **2011,** *133*, 8444-8447.

25. Gagnon, Y. J.; Roth, C. B., Local Glass Transition Temperature $T_g(z)$ Within Polystyrene Is Strongly Impacted by the Modulus of the Neighboring PDMS Domain. *ACS Macro Lett.* **2020,** *9*, 1625-1631.

26. Hao, Z.; Ghanekarade, A.; Zhu, N.; Randazzo, K.; Kawaguchi, D.; Tanaka, K.; Wang, X.; Simmons, D. S.; Priestley, R. D.; Zuo, B., Mobility gradients yield rubbery surfaces on top of polymer glasses. *Nature* **2021,** *596*, 372-376.

27. Qi, D.; Fakhraai, Z.; Forrest, J. A., Substrate and Chain Size Dependence of Near Surface Dynamics of Glassy Polymers. *Phys. Rev. Lett.* **2008,** *101*, 096101.

28. Burroughs, M. J.; Napolitano, S.; Cangialosi, D.; Priestley, R. D., Direct Measurement of Glass Transition Temperature in Exposed and Buried Adsorbed Polymer Nanolayers. *Macromolecules* **2016,** *49*, 4647-4655.

29. Fakhraai, Z.; Forrest, J. A., Measuring the Surface Dynamics of Glassy Polymers. *Science* **2008,** *319*, 600-604.

30. Zuo, B.; Qian, C.; Yan, D.; Liu, Y.; Liu, W.; Fan, H.; Tian, H.; Wang, X., Probing Glass Transitions in Thin and Ultrathin Polystyrene Films by Stick–Slip Behavior during Dynamic Wetting of Liquid Droplets on Their Surfaces. *Macromolecules* **2013,** *46*, 1875-1882.

31. Keddie, J. L.; Jones, R. A. L.; Cory, R. A., Interface and Surface Effects on the Glass-transition Temperature in Thin Polymer Films. *Faraday Discuss.* **1994,** *98*, 219–230.

32. Eisenberg, A., Glass transitions in ionic polymers. *Macromolecules* **1971,** *4*, 125-128.

33. Mckague, E. L.; Reynolds, J. D.; Halkias, J. E., Swelling and glass transition relations for epoxy matrix material in humid environments. *J. Appl. Polym. Sci.* **1978,** *22*, 1643-1654.

34. Bicerano, J.; Sammler, R. L.; Carriere, C. J.; Seitz, J. T., Correlation between glass transition temperature and chain structure for randomly crosslinked high polymers. *J. Polym. Sci., Part B: Polym. Phys.* **1996,** *34*, 2247-2259.

35. Rittigstein, P.; Priestley, R. D.; Broadbelt, L. J.; Torkelson, J. M., Model polymer nanocomposites provide an understanding of confinement effects in real nanocomposites. *Nat. Mater.* **2007,** *6*, 278–282.

36. Wang, H.; Hor, J. L.; Zhang, Y.; Liu, T.; Lee, D.; Fakhraai, Z., Dramatic Increase in Polymer Glass Transition Temperature under Extreme Nanoconfinement in Weakly Interacting Nanoparticle Films. *ACS Nano* **2018,** *12*, 5580-5587.

37. Maguire, S. M.; Bilchak, C. R.; Corsi, J. S.; Welborn, S. S.; Tsaggaris, T.; Ford, J.; Detsi, E.; Fakhraai, Z.; Composto, R. J., Effect of Nanoscale Confinement on Polymer-Infiltrated Scaffold Metal Composites. *ACS Appl. Mater. Interfaces* **2021,** *13*, 44893-44903.

38. Hor, J. L.; Wang, H.; Fakhraai, Z.; Lee, D., Effect of Physical Nanoconfinement on the Viscosity of Unentangled Polymers during Capillary Rise Infiltration. *Macromolecules* **2018,** *51*, 5069-5078.

39. Hor, J. L.; Wang, H.; Fakhraai, Z.; Lee, D., Effects of polymer–nanoparticle interactions on the viscosity of unentangled polymers under extreme nanoconfinement during capillary rise infiltration. *Soft Matter* **2018,** *14*, 2438-2446.

40. Porter, C. E.; Blum, F. D., Thermal Characterization of PMMA Thin Films Using Modulated Differential Scanning Calorimetry. *Macromolecules* **2000,** *33*, 7016-7020.

41. Efremov, M. Y.; Olson, E. A.; Zhang, M.; Zhang, Z.; Allen, L. H., Glass Transition in Ultrathin Polymer Films: Calorimetric Study. *Phys. Rev. Lett.* **2003,** *91*, 085703.

42. Park, J.; Han, S.; Park, H.; Lee, J.; Cho, S.; Seo, M.; Kim, B. J.; Choi, S. Q., Simultaneous Measurement of Glass-Transition Temperature and Crystallinity of As-Prepared Polymeric Films from Restitution. *Macromolecules* **2021,** *54*, 9532-9541.

43. Palade, L. I.; Verney, V.; Attane, P., Time-temperature superposition and linear viscoelasticity of polybutadienes. *Macromolecules* **1995,** *28*, 7051-7057.

44. Higgenbotham-Bertolucci, P. R.; Gao, H.; Harmon, J. P., Creep and stress relaxation in methacrylate polymers: Two mechanisms of relaxation behavior across the glass transition region. *Polym. Eng. Sci.* **2001,** *41*, 873-880.

45. Fakhraai, Z.; Forrest, J. A., Probing Slow Dynamics in Supported Thin Polymer Films. *Phys. Rev. Lett.* **2005,** *95*, 025701.

46. Lupaşcu, V.; Picken, S. J.; Wübbenhorst, M., Cooperative and non-cooperative dynamics in ultra-thin films of polystyrene studied by dielectric spectroscopy and capacitive dilatometry. *J. Non-Cryst. Solids* **2006,** *352*, 5594-5600.

47. Boucher, V. M.; Cangialosi, D.; Yin, H.; Schönhals, A.; Alegría, A.; Colmenero, J., T_g depression and invariant segmental dynamics in polystyrene thin films. *Soft Matter* **2012,** *8*, 5119-5122.

48. Perez-de-Eulate, N. G.; Di Lisio, V.; Cangialosi, D., Glass Transition and Molecular Dynamics in Polystyrene Nanospheres by Fast Scanning Calorimetry. *ACS Macro Lett.* **2017,** *6*, 859-863.

49. Rosa, A. C. P.; Cruz, C.; Santana, W. S.; Brito, E.; Moret, M. A., Non-Arrhenius behavior and fragile-to-strong transition of glass-forming liquids. *Phys. Rev. E* **2020,** *101*.

50. Xie, R.; Weisen, A. R.; Lee, Y.; Aplan, M. A.; Fenton, A. M.; Masucci, A. E.; Kempe, F.; Sommer, M.; Pester, C. W.; Colby, R. H.; Gomez, E. D., Glass transition temperature from the chemical structure of conjugated polymers. *Nat. Commun.* **2020,** *11*, 893.

51. Angelescu, D. E.; Waller, J. H.; Adamson, D. H.; Deshpande, P.; Chou, S. Y.; Register, R. A.; Chaikin, P. M., Macroscopic Orientation of Block Copolymer Cylinders in Single-Layer Films by Shearing. *Adv. Mater.* **2004,** *16*, 1736–1740.

52. Davis, R. L.; Chaikin, P. M.; Register, R. A., Cylinder Orientation and Shear Alignment in Thin Films of Polystyrene–Poly(*n*-hexyl Methacrylate) Diblock Copolymers. *Macromolecules* **2014,** *47*, 5277–5285.

53. Kim, Y. C.; Kim, D. H.; Joo, S. H.; Kwon, N. K.; Shin, T. J.; Register, R. A.; Kwak, S. K.; Kim, S. Y., Log-Rolling Block Copolymer Cylinders. *Macromolecules* **2017,** *50*, 3607–3616.

54. Kim, D. H.; Kim, S. Y., Universal Interfacial Control through Polymeric Nanomosaic Coating for Block Copolymer Nanopatterning. *ACS Nano* **2020,** *14*, 7140–7151.

55. Kim, S. E.; Kim, D. H.; Kim, S. Y., Facile and Fast Interfacial Engineering Using a Frustrated Interfacial Self-Assembly of Block Copolymers for Sub-10-nm Block Copolymer Nanopatterning. *Adv. Funct. Mater.* **2022,** *32*, 2202690.

56. Kim, K. D.; Sperling, L. H.; Klein, A.; Hammouda, B., Reptation Time, Temperature, and Cosurfactant Effects on the Molecular Interdiffusion Rate during Polystyrene Latex Film Formation. *Macromolecules* **1994,** *27*, 6841-6850.

57. Zhang, C.; Cavicchi, K. A.; Li, R.; Yager, K. G.; Fukuto, M.; Vogt, B. D., Thickness Limit for Alignment of Block Copolymer Films Using Solvent Vapor Annealing with Shear. *Macromolecules* **2018,** *51*, 4213-4219.

58. Lin, Y. H., Entanglement and the molecular weight dependence of polymer glass transition temperature. *Macromolecules* **1990,** *23*, 5292-5294.

59. Fox, T. G.; Flory, P. J., The glass temperature and related properties of polystyrene. Influence of molecular weight. *J. Polym. Sci.* **1954,** *14*, 315-319.

60. Sharp, J. S.; Forrest, J. A., Free Surfaces Cause Reductions in the Glass Transition Temperature of Thin Polystyrene Films. *Phys. Rev. Lett.* **2003,** *91*, 235701.

61. Fakhraai, Z.; Sharp, J. S.; Forrest, J. A., Effect of sample preparation on the glass-transition of thin polystyrene films. *J. Polym. Sci., Part B: Polym. Phys.* **2004,** *42*, 4503-4507.

62. Ma, Z.; Nie, H.; Tsui, O. K. C., Substrate influence on the surface glass transition temperature of polymers. *Polymer* **2024,** *312*, 127594.

63. Chai, Y.; Salez, T.; Mcgraw, J. D.; Benzaquen, M.; Dalnoki-Veress, K.; Raphaël, E.; Forrest, J. A., A Direct Quantitative Measure of Surface Mobility in a Glassy Polymer. *Science* **2014,** *343*, 994-999.

64. Wang, H.; Kearns, K. L.; Zhang, A.; Arabi Shamsabadi, A.; Jin, Y.; Bond, A.; Hurney, S. M.; Morillo, C.; Fakhraai, Z., Effect of Nanopore Geometry in the Conformation and Vibrational Dynamics of a Highly Confined Molecular Glass. *Nano Lett.* **2021,** *21*, 1778-1784.

65. Ren, T.; Hinton, Z. R.; Huang, R.; Epps, T. H.; Korley, L.; Gorte, R. J.; Lee, D., Increase in the effective viscosity of polyethylene under extreme nanoconfinement. *J. Chem. Phys.* **2024,** *160*.

The source data are also available via Figshare at https://doi.org/10.6084/m9.figshare.26073427